The investigation of mechanical and thermal properties of super-hydrophobic nitinol surfaces fabricated by hybrid methods of laser irradiation and carbon ion implantation

Meng Wang[a,b], *Zhen Yang*[a,b,c], *Chengjuan Yang*[a,b*], *Dawei Zhang*[a,b], *Yanling Tian*[a,b,c], *Xianping Liu*[c]

[a] School of Mechanical Engineering, Tianjin University, Tianjin 300054

[b] Key Laboratory of Mechanism Theory and Equipment Design of Ministry of Education, Tianjin 300072, China

[c] School of Engineering, University of Warwick, Coventry CV4 7AL, UK

Abstract

Comparing with laser irradiation only, the laser ablation combined with chemical modification process is a widely used technique to obtain bio-inspired super-hydrophobic surface. However, the as-prepared surfaces may be polluted by toxic substance during chemical modification such as fluoroalkyl silane and stearic acid. The side effect of polluted functional surface on organisms and environment limited its application value. In this paper, a green and environmental-friendly super-hydrophobic surface was quickly fabricated on nitinol substrates through hybrid of nanosecond laser ablation and carbon ion implantation. The time that turning from super-hydrophilicity to super-hydrophobicity was only 16 hours exhibiting high efficiency compared with pure laser processing. Surface morphology and chemical component were systematically investigated to reveal the formation mechanism of super-hydrophobicity in such short time. The mechanical abrasion tests implied that the mechanical properties of surface microstructure could be heightened after carbon ion implantation, showing the superior structure stability. It is noted that chemical modified super-hydrophobicity could be hardly destroyed under high temperature, and the thermal stability of this ion implanted super-hydrophobic surface was on a par with it. This hybrid method of laser irradiation and carbon ion implantation paves a green way for rapid fabrication super-hydrophobic surface on nitinol, which would have great application value in biomedicine and industry.

* Corresponding author at: School of Mechanical Engineering, Tianjin University, Tianjin 300500, China.
E-mail address: cjytju@tju.edu.cn

Keywords: Wettability; Transformation time; Carbon ion implantation; Laser texturing; Abrasion stability; Thermal stability

1. Introduction

Learning from nature is a significant fountainhead of emerging technology and advanced materials [1]. Some natural plants and animals have developed specific functional surface to acclimatize themselves to extreme environments. Lotus leaves prevent the dust from adsorbing on them exhibiting self-cleaning character [2-3] and the desert beetles rely on their shell harvesting water surviving in arid environment [4]. Previous literatures have reported that super-hydrophobic phenomenon, where the surface water contact angel is greater than 150°, exhibits unique properties, including self-cleaning, corrosion inhibition, anti-bacteria, oil/water separation and drag reduction [5-13]. However, these kinds of special performances would lose efficacy under extreme environment (high temperature or friction) due to the poor stability, which limits the practical application very much. Hence, a great deal of theoretical research about improving the stability of hydrophobic surface has been carried out to develop its potential application [14].

Due to the huge potentials in practice, multifarious of techniques have been explored to successfully fabricate bio-inspired super-hydrophobic surface, including chemical vapor deposition, self-assembly, chemical etching, electrospinning, sol-gel, anodic oxidation, and spin coating [15-21]. However, the mentioned approaches involving easy-falling of fabricated micro-nano structure, complicated fabricating process and high cost severely limit their application. Conversely, laser texturing method has been reported as a high-efficiency, convenient and green approach to produce super-hydrophobic surfaces [22]. Besides, the controllable surface photography can be obtained via setup laser processing parameters [23-25]. Therefore, laser processing method was employed in this study. The research about hydrophobic surface has been carried on many kinds of materials, including metals, ceramics, and high-molecular polymer. Among above mentioned materials, titanium alloy, as a newly developed materials has drawn huge attentions due to its special performance such as wear resistance [26], super-elasticity [27], shape memory effect (SME) [28] and biocompatibility [29-30]. It has wide applications in medicine, biology, aerospace, and Micro Electric Mechanical System (MEMS) [31]. Thereby,

wettability modification of titanium alloy has become one of hot research topics. Though the phenomenon of nickel ion release into vivo exists in the NiTi alloys, it causes no harm to human health because the amount of released nickel ion is extraordinary few. Hence, NiTi alloys are still the perfect materials for fabricating implant medical device in medicine such as dental prostheses and cardiac valves. They are also employed for manufacturing orthopedic devices. Nevertheless, the performance of medical implants will be adversely affected by the presence of bacterial biofilms which can give rise to infection [32]. The absorption of this kind human pathogenic biofilms on the medical implant surface is one of the primary causes of the failure of surgery operation, resulting in the necessity of removing the implants even being associated with systemic infection, which causes the amputation or death [33]. The research about removing the biofilms from indwelling devices is of great significance [34]. Super-hydrophobic surface has great application value in this filed due to its anti-bacteria performance. The super-hydrophobic surface can be generally obtained via processing hierarchical structure and modifying low surface energy chemical materials. However, the modification process may cause harm to human body due to the perniciousness of chemical materials, which brings about the urgent needs of green and health method (without chemical modification process) to prepare super-hydrophobic surface [35]. Elena et al., fabricated the two-tier micro and nanoscale quasi-periodic self-organized structures with the large grain-like convex features below 20 μm and bulges about 200 nm using femtosecond laser ablation. The hierarchical structure enhanced the ability of hydrophobicity and the ablated surface showed super-hydrophobic performance with the WCA of 166±4 ° even without any other chemical modification. They investigated the interaction of S. aureus and P. aeruginosa with the super-hydrophobic surface at the solid liquid interface and the result revealed that the fabricated surface exhibited a highly selective retention ability for the two pathogenic bacteria. Any kind of adsorbed bacterial cells maintained the situation in which the attached value was under the estimated detection limit [36]. Specifically, the titanium is also an ideal material as power-intensive energy components and titanium-based composites including heat pumps, heat exchanger of aircraft and aerospace due to its light weight, high mechanical strength and corrosion-resistant performance. The super-hydrophobic surface has been widely used in the cooling system of spacecraft [37]. It is significant to ensure the super-hydrophobicity survive under the attack of high temperature. The

Jumping Droplet Thermal Diode (JDTD) [38], as a recently invented technology is a desirable spacecraft thermal control [39]. A super-hydrophobic wick is the important components of JDTD where the working fluid dislodged the heat and evaporates. Jacob et al. [40] modified the surface morphology by femtosecond laser on titanium substrates and lower its surface energy through immersion into fluorinated silane, vapor deposition of fluorinated silane, and grafting of PDFA, respectively. They carried out the thermal cycle testing on three different super-hydrophobic surfaces and all of them survived through the temperature range of -30 ℃ to 70 ℃. Titanium with functional surface is also widely used in industry [41], micro-electronics [42] and construction [43]. However, this functional surface is out of use once surface is destroyed. Therefore, improving the abrasion stability of hydrophobicity surface is of common interest. Xiao et al. fabricated robust hydrophobic surface through liquid-phase laser ablation with the WCA of 148.4±0.6 ° and WSA of 4.5±0.5 °, respectively. They found that the hydrophobic surface fabricated by liquid-phase laser ablation showed better abrasion stability and hydrophobicity after being worn by hand-polishing 600 times on 1200 grid sandpaper.

Ion implantation is a widely used surface modification method. Xia et al. [44], implanted carbon ions into titanium surface by plasma immersion ion implantation and deposition (PIII&D) technology, which enhanced the mechanical property. However, there is an absence of relevant report about investigating the relationship between carbon ion implantation modification and surface wettability. In this paper, a novel facial method, injecting carbon ion on nanosecond laser ablated surface was proposed to rapidly fabricate hierarchical super-hydrophobic surface without any other chemical modification. The surface wettability transforming from super-hydrophilicity to super-hydrophobicity only needs 16 hours. This method presents vital advantages regarding low-cost, convenient and efficient comparing with other fabricating hierarchical super-hydrophobic surface methods, such as fabricating hierarchical superimposed nano-microstructure by femtosecond and assembly from colloidal system [45]. It is worth emphasizing that no harmful substances participate the preparation process, and therefore it has great application in medicine. The stability of super-hydrophobic surface has drawn extensive concern based on which, the effects of carbon ion implantation on thermal stability and abrasion stability were investigated in this study. Furthermore, the mechanism of thermal

stability and abrasion stability of modified surface was also discussed to make a better understanding of the stability of hydrophobic surface, which will raise the promising prospects of applications for nitinol material.

2 Experiment method

2.1 Materials and chemicals

Experiments were performed on nitinol alloy with the size of Φ20 mm × 1 mm (chemical components: Ni 50% and Ti 50%), provided by Yipinchuancheng (Beijing) Technology Co. Ltd. The ethanol (AR, 95%) were purchased from Alfa Aesar. The acetone (AR, ＞99.5 %) were provided by Jiangtian Chemical Technology Co. Ltd. Before the laser ablation process, all the samples were mechanically polished by a high-speed polishing machine until obtaining mirror surface, following with the cleaning processes in acetone (AR, ＞99.5%), ethanol (AR, 95%) and distilled water each for 10 min using the ultrasonic cleaning tank. Finally, all the rinsed samples were dried under high-purity nitrogen gas.

2.2 Laser patterning

The prepared samples were irradiated by Ytterbium nanosecond pulsed fiber laser system (IPG photonics from Germany) at atmospheric environment with processing parameter exhibited in Table 1. As shown in Fig. 1(a), grid microstructure with the size of 80 μm × 80 μm was fabricated under the irradiation of laser beam and the scanning period of laser beam is defined as the distance between the middle lines of two adjacent grooves.

Table 1. Laser processing parameters.

Laser parameter	Symbol (unit)	Values
Wavelength	λ *(nm)*	1064
Pulse duration	τ *(ns)*	50
Repetition rate	*f (kHz)*	20
Spot diameter	Φ *(μm)*	50
Average power	*P (W)*	15
Scanning speed	$V\ (mm{\cdot}s^{-1})$	300

2.3 Carbon ion implantation

Ion implantation of carbon element was carried out on a MT3-R2 ion implanter and the accelerating voltage was set at 40 kV in a high vacuum condition (< 10^{-3} Pa) at room temperature. The variable content of carbon ions was set as 1×10^{17} ions/cm^2. The laser processed samples were divided into two group according to whether carbon ion was injected or not. L: The samples were purely irradiated by nanosecond laser without any other treatment; LI: The samples were ablated by nanosecond laser followed by carbon ion implantation immediately.

3 Testing Method

3.1 Surface characterization

To investigate the effects of laser ablation and carbon ion implantation on surface wettability, water contact angles (WCAs) and water sliding angles (WSAs) of two kinds of samples were measured on a water contact angle goniometer (AST, VCA optima). Besides, surface microstructures of the treated samples were observed through scanning electron microscope (SEM: FEI, Quanta 250 FEG) and Leica microscope. 3D profiles and surface roughness were evaluated by a white confocal light microscope (CountourGT, Bruker). X-ray photoelectron spectroscopy (XPS: Thermo Fisher Scientific, Escalab 250Xi) was used to analyze the surface chemical compositions.

3.2 Thermal stability experiment

To investigate the thermal stability of fabricated surface, L and LI samples were heated in a heating furnace under aerobic environment. Heating-process was carried out under the temperature ranging from 50 ℃ to 950 ℃ with a climbing step of 50 ℃. The samples were kept in the heating furnace for 30 min at each target temperature. After the heat treatment, the samples were cooled vacuum environment, followed by blown under high-purity nitrogen gas.

3.3 Abrasion stability experiment

The abrasion stability of L and LI samples were assessed by sandpaper abrasion test. A weight of 200g and a 1500 grid sandpaper with the size of 30 cm both in length and width were main testing apparatus. During abrasion test, the modified surface contacted with the sandpaper with a 200 g weight pressing on sample. An abrasion cycle was obtained when moving the sample 25 cm in one direction, then moving back in the opposite direction at a constant rate of 20 mm/s. The worn samples were cleaned in deionized water and dried under high-purity nitrogen gas after each of the abrasion cycle.

4 Results and discussion

4.1 Analysis of surface morphology

4.1.1 Effect of laser irradiation on surface morphology

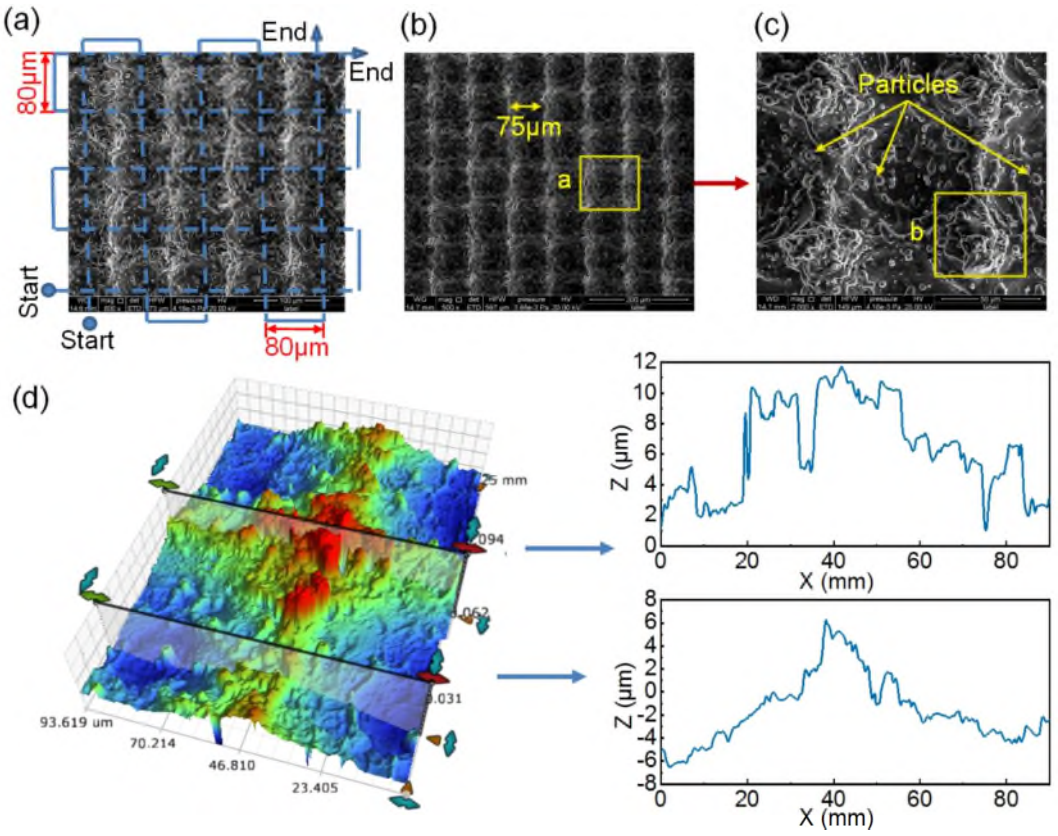

Figure 1. Variation of surface morphology induced by laser ablation process.

3D profiles and surface topography were shown in Fig. 1. According to the processing path in Fig. 1 (a), laser ablated surface was bestrewed with grid pattern with the basin-shaped pits, ridges and protrusions as shown in Fig. 1 (c), which were visible under magnification 3D profiles of Fig. 1 (d). The line-by-line laser scanning with period of 80 μm (almost equal to the width of laser irradiated grooves of 75 μm) was carried out along the vertical directions, which leads to the formation of periodic rosette protrusions (area b in Fig. 1 (c)). The laser ablated material experienced melting, splashing and condensing, as a result, particles irregularly deposited on the inside wall and the brim of grooves in Fig. 1 (c).

To further investigate the mechanism of laser ablation on sample surface, the enlarged 3D profiles of the basic unit were analyzed in Figs. 1 (d). According to enlarged 3D profiles, the altitude of the

laser-induced surface varied significantly containing three kinds of morphologies: basin-shaped pits with the altitude of -6 μm, ridges with the altitude of 5 μm and protrusions with the altitude of 11 μm. Obviously, the protrusion had the highest altitude, followed by the ridge, and the pits had the smallest altitude. This is due to the different overlap of laser scanning strategy. Previous reports have proved that grooves will generated on laser abated area and the ridge will form on the brim of the grooves due to the accumulation of exceeded materials. In Fig. 1 (d), the basin-shape pits experienced twice laser scanning and none accumulation of ejected material, while the ridges experienced once laser scanning and twice accumulation of ejected material. However, the protrusions experienced four times accumulation and never underwent any laser scanning. Therefore, the altitudes of pits, ridges and protrusions were significantly distinct.

4.1.2 Effect of carbon ion implantation on surface morphology

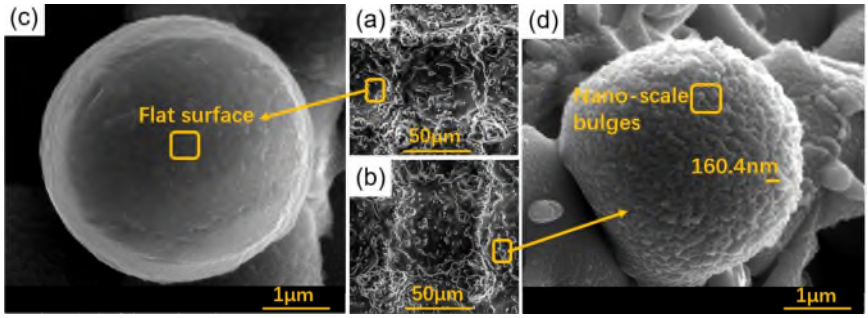

Figure 2. SEM images of (a) grid element and (c) particles on L samples surface; SEM images of (b) grid element and (d) particles on LI samples surface

In Figs. 2 (a) and (b), regular grid patterns with micron-scale ridges, rosette protrusions and pits formed on both of L and LI wafer surfaces. And all of these microstructures were decorated with irregular micro droplet shaped particles. Hence, it indicated that carbon ion implantation can't change the surface morphology on micron scale. Further observation from Fig. 2 (d), the surface morphology on nano-scale of LI samples changed obviously and a large amount of nanoscale bulges ranged from 100nm to 300nm (the lotus-leaf-like hierarchical structures) can be seen on micron particles' surfaces. However, Fig. 2 (c) exhibited the flat surface. Therefore, it makes sense that surface roughness obviously increased after carbon ion implantation as shown in Table 2.

Table 2. Surface roughness of L and LI samples.

Sample	L	LI
Roughness	8.360	9.312

4.2 Analysis of surface wettability

Figs. 3 (a) and (b) revealed the revolution of surface wettability with time in atmospheric environment for L and LI samples, respectively. Before laser processing, the pure NiTi alloy showed intrinsic hydrophilicity with WCA value of 68.2±2.3 °. According to Fig. 3 (a), immediately after laser processing, the samples showed high hydrophilicity with WCAs of 0 °. This phenomenon well maintained within four days. Ten days later, the WCAs rose to 50 ° by inches. Then, a sharp increase appeared with WCAs ranging from 130 ° to 140 °. After 20 days, surface wettability reached the steady stage fluctuating around 145°. During the whole measurement process, all water droplets were stuck onto the laser treated surface firmly even the wafers were turned upside down. As far as LI samples, the time transforming from hydrophilicity to super-hydrophobicity was only 16 hours in Fig. 3 (b). After the hybrid of laser processing and carbon ion implantation, the WCAs witnessed a steady increase from 0 ° to more than 150 ° within 14 hours. WSAs remained 180 ° in the first 12 hours and then sharply doped to 3.2 ° within four hours. Exhilaratingly, the WCAs exceeded 150 ° and the WSAs went down below 10 °, which can be regarded as a typical super-hydrophobic surface after being exposed in clean ambient air for 16 hours.

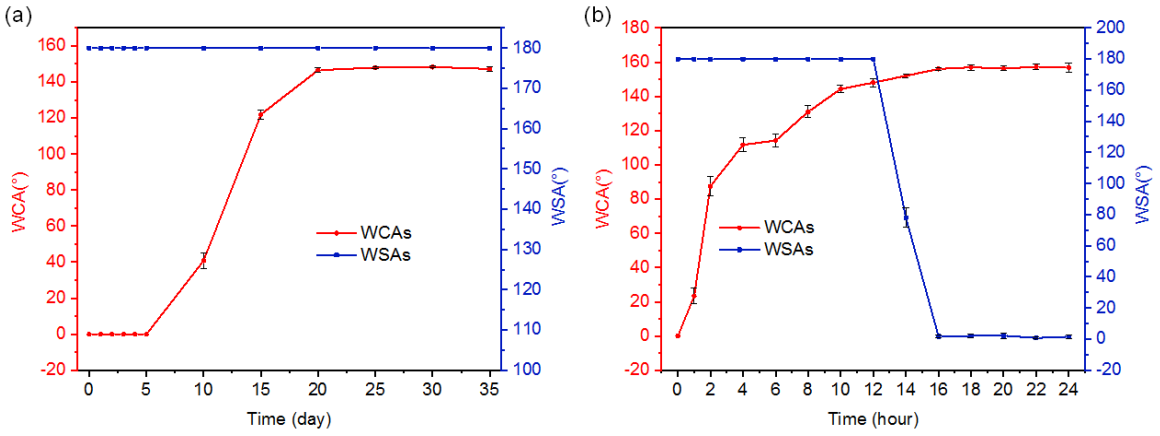

Figure 3. The revolution of WCAs for (a) L and (b) LI samples with time in ambient air.

According to Fig. 3, carbon ion implantation process distinctly accelerated the transformation process from hydrophilicity to hydrophobicity or even super-hydrophobicity. As far as L samples, the transformation process took 20 days. However, LI wafers only spent 16 hours. Besides, surface hydrophobicity of LI samples was obviously enhanced presenting typical super-hydrophobic surface. According to Wenzel theory [46], hydrophilic surface would become more hydrophilicity and hydrophobic surface would become more hydrophobic with the increase of surface roughness. The wettability of LI samples conformed to the Wenzel model because the increase of surface roughness resulted in the increase of WCAs value. Fig. 4 further exhibited the mechanism of this phenomenon. A great deal of nanoscale bulges ranging from 100 nm to 300 nm appeared on the surface of drop-like micro particles and the hierarchical micro/nano structure was obtained through the modification process of ion implantation. Therefore, the compound solid-air-liquid interface was formed when the liquid droplet get in touch with the hierarchical microstructure and the multi-scale air pocket were trapped underneath the droplet. The adhesion of droplet to solid surface obviously weakened because the contact area between liquid and solid decreased, as a result, the WSAs decreased [47].

Carbon ion implantation combined with laser irradiation is a newly high-efficiency method to prepare super-hydrophobic surface. As we all know, both of the surface morphology and surface chemical composition play the important roles on surface wettability. To make certain the relationship between carbon ion implantation and surface wettability, it is necessary to investigate the influence of carbon ion implantation on surface chemical compositions further.

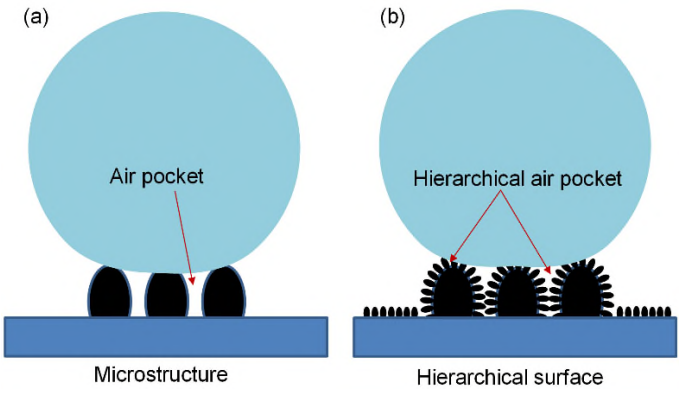

Figure 4. Schematic of droplet on the surfaces respectively with single microstructures and hierarchical microstructures.

4.3 Analysis of chemical composition

4.3.1 Chemical composition analysis

Fig. 5 demonstrated the XPS spectra of fresh L samples (a), 35-day air exposed L samples (b), fresh LI samples (c) and 16-hours exposed LI samples (d), respectively. According to the result, the texted surface contained four essential elements: The C 1s at 285.0 eV, Ti 2p at 475.0 eV, O 1s at 545.0 eV and Ni 2p at 888.0 eV. On account of extremely low content, other elements were ignored and we only exhibited the bonding energy ranging from 200 eV-900 eV in XPS spectra. By analyzing the XPS result, an inference can be obtained that the titanium and nickel primarily existed in the form of titanium oxide and nickel oxide, respectively. As shown in Fig. 5 (a), if the fresh L samples were clean enough and free of pollution, the carbon contents should be zero. However, the high-resolution of C 1s spectra results demonstrated that carbonaceous matter was detected on fresh L samples surface. The redundant carbonaceous matter came from two main source: the adhesion of airborne organic matters during the period from fabricating process to XPS examination and the volatile oil in vacuum chamber of XPS instrument. As far as fresh LI samples, the carbon contents would increase in the same way. Besides, the injected carbon ion is another main source. According to Fig. 5, it can be found that the carbon contents witnessed the increase trend when the samples being exposed in ambient air. Previous literature has revealed that the transformation of surface wettability with time was owe to the adsorption of organic matter on surface.

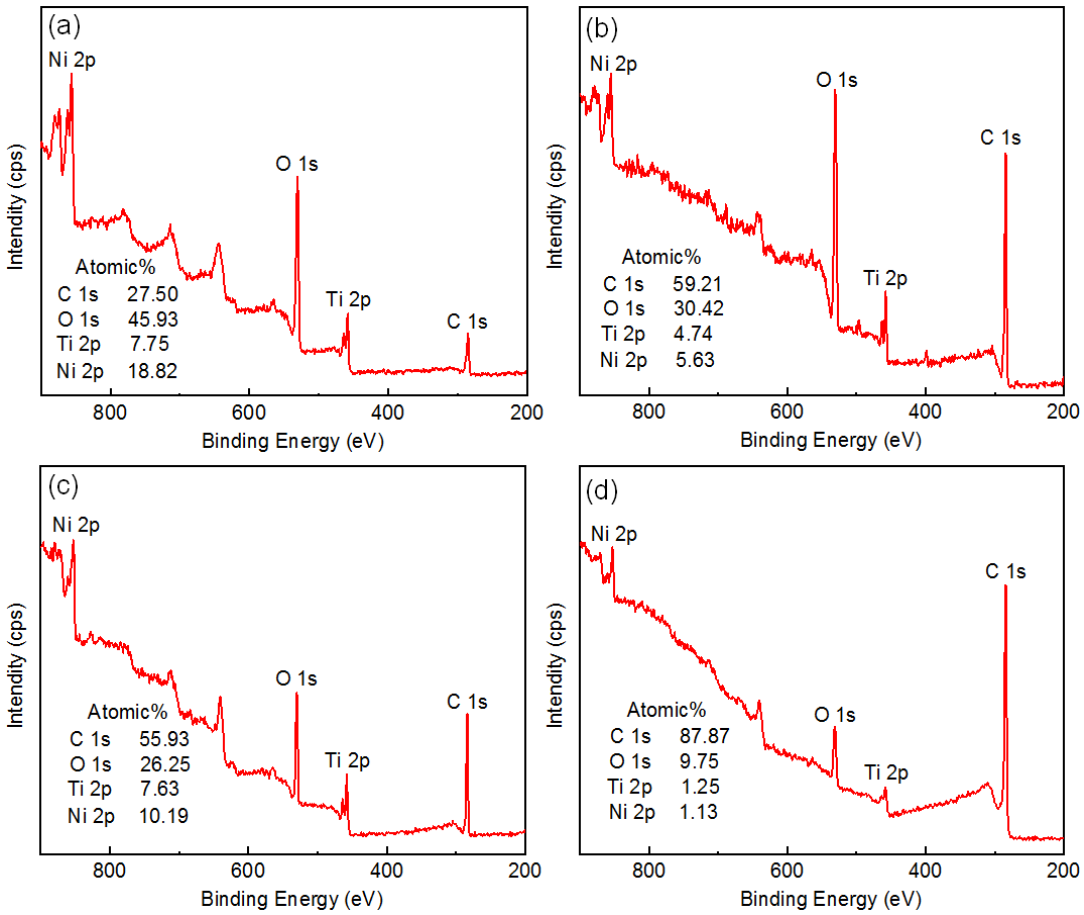

Figure 5. XPS spectra of (a) fresh L samples; (b) 35-day air exposed L samples; (c) fresh LI samples and (d) 24-hours exposed LI samples.

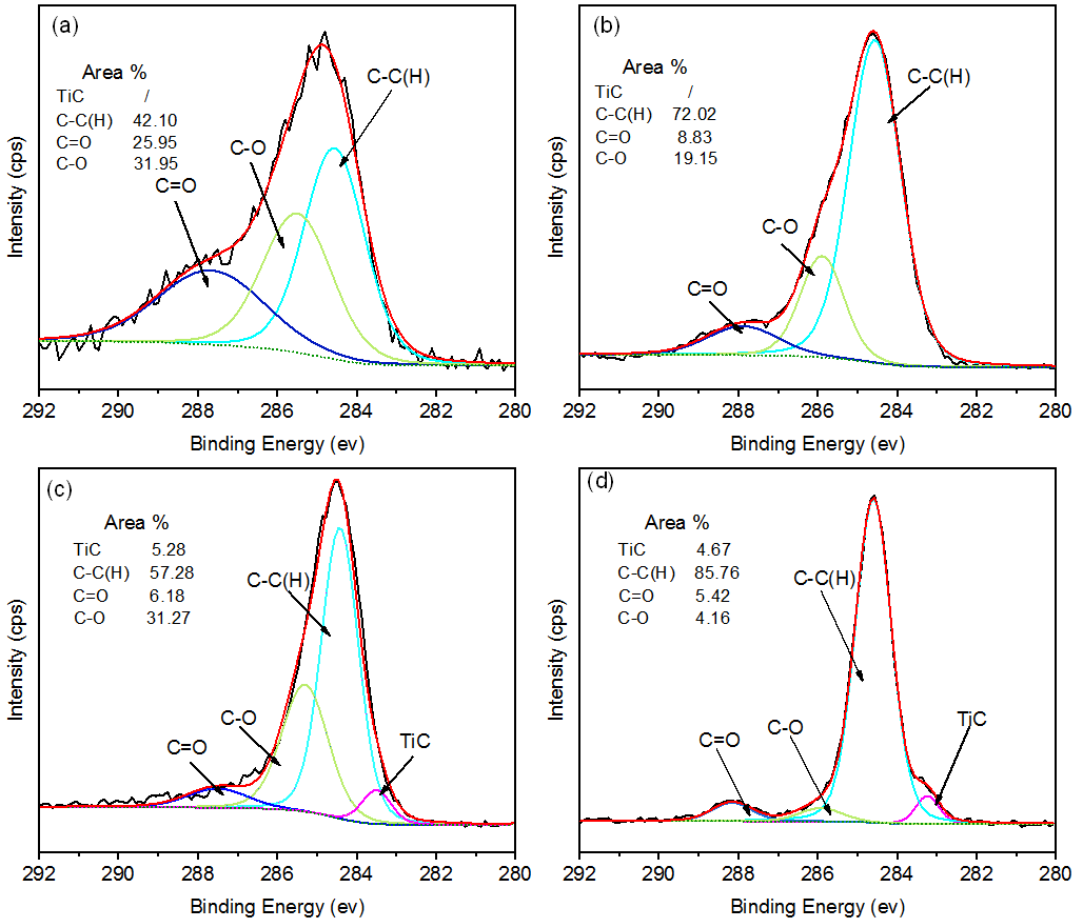

Figure 6. The high-resolution of C 1s spectra on fresh L samples (a), 35-day exposed L samples (b), fresh LI samples (c), and 24-hours exposed LI samples (d).

To reveal the transformation mechanism of surface wettability on L and LI samples, the corresponding high-resolution of C 1s spectra of the investigated samples was shown in Fig. 6. According to Figs. 6 (a) and (b), the C 1s peak was disassembled into three components. The peak located at 284.5 eV, 285.5 eV and 287.7 eV were regarded as the function group C-C(H), C-O and C=O respectively. As far as NiTi alloy, titanium oxide and nickel oxide were generated with a great deal of atoms in the form of Ti^{2+}, Ni^{2+} and O^{2-} after laser processing [48]. The metallic oxide showed hydrophilicity due to the undersaturated titanium, nickel and oxygen atoms serving as Lewis acid and base pairs [49]. The titanium and nickel atoms were electron-deficient with only four and six electrons in sp^{2-} hybrid orbitals, respectively. These atoms captured the hydrogen bonds from water molecules to obtain a full octet electron [50] as shown in Fig. 7. Hence, the fresh laser ablated surface emerged high surface polarity with extremely non-equilibrium, resulting in the presence of super-hydrophilicity.

The high-resolution of C 1s spectra witnessed a sharp increase for C-C(H) functional group from 42.10 % to 72.01 % after the L samples being exposed in ambient air for 35 days, indicating the chemisorption of organic matters such as formic and acetic acid in the air onto laser ablated surface. The relevant chemical reaction process was presented in Eq. (1) and the relevant reaction process was demonstrated in Fig. 8.

$$Ni - OH + RCOOH \rightarrow RCOO - Ni + H_2O \quad (1)$$

$$Ti - OH + RCOOH \rightarrow RCOO - Ti + H_2O$$

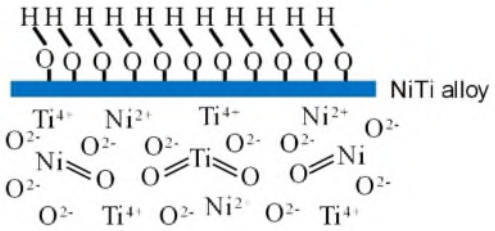

Figure 7. Schematic illustration of hydroxylation process of laser ablated surface.

The carboxylates in the air including formic and acetic acid were chemisorbed onto laser processed surface via dehydration reaction with attached hydroxyls. As a result, the chain R containing nonpolar groups C-C(H) was chemisorbed onto the surface layer in forms of nickel salt and titanium salt, which acutely lowered the surface energy. This depolarization procedure was sluggish accounting for the piecemeal transformation from hydrophilicity to hydrophobicity.

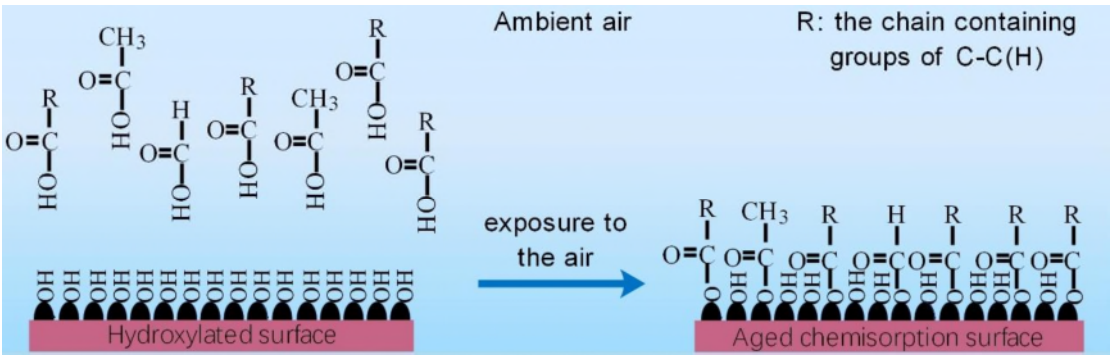

Figure 8. Schematic illustration of chemisorption process.

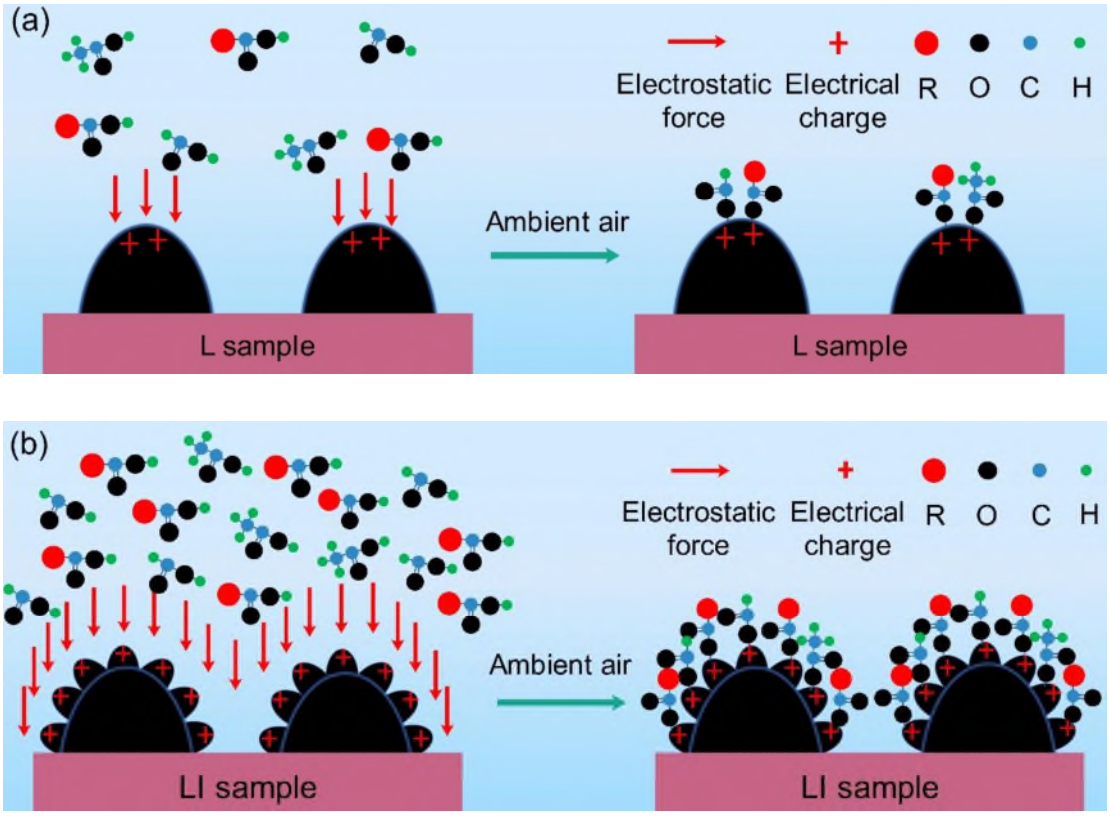

Figure 9. Adsorption mechanism of L (a) and LI (b) samples.

Figs. 6 (c) and (d) clearly demonstrated that C 1s spectra of carbon ion implanted surface consisted of four main components: C=O at 287.6 eV, C-O at 285.6 eV, C-C(H) at 284.6 eV and TiC at 283.2 eV. Compared with L samples surface, it is obvious that TiC was generated after carbon ion implantation. When the carbon ion implanted samples were exposed into ambient air for more than 16 hours, the nonpolar group C-C(H) presented a prominent increase from 57.28 % to 85.76 %. In the same way, the LI samples experienced hydration and chemisorbing carboxylates procedure during the transition from super-hydrophilicity to super-hydrophobicity as shown in Fig. 8. Compared with L samples, the super-hydrophobicity derived from two main causes: more attached nonpolar group C-C(H) and TiC possessing the low surface free energy of 44.49 $mJ \cdot m^{-2}$ -55.12 $mJ \cdot m^{-2}$ at room temperature [51]. Besides, the transform time was sharply reduced in terms of LI samples, owing to the appearance of lotus-leaf-like hierarchical structures as shown in Fig. 4 (b). Just like vesicular structure resulting in adsorptive property of activated carbon [52], the vesicular structure formed after carbon ion implantation also presented superior adsorption performance. According to the adsorption

electrostatic principle [53], this kind surface was electriferous due to the adsorption of charge from air. Tip discharge principle has revealed that, in terms of sharp object, a great deal of charge easily assembled on the cusp, resulting in the generation of electrostatic force [54]. Fig. 9 further revealed the mechanism of this phenomenon. Nanoscale bulges generated on micron particle surfaces could gather with a great deal of charge, which enhancing the adhering of carboxylates in the air in terms of velocity and quantity. Besides, the area exposed to the air increased, which can accommodate more nonpolar chain.

4.3.2 Chemical composition analysis about nanoscale bulge

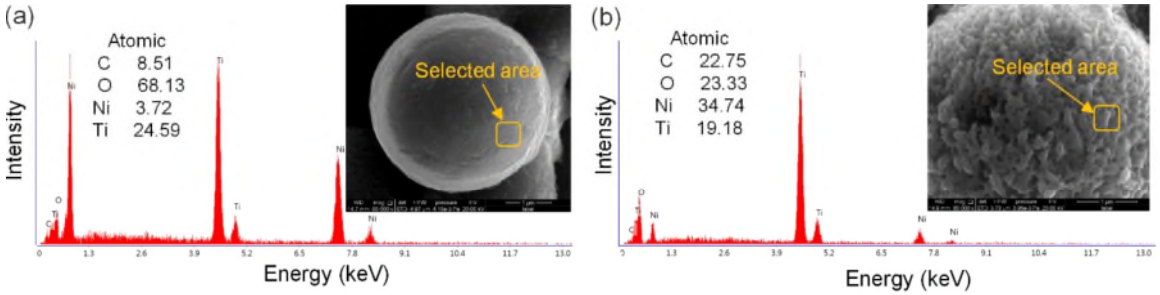

Figure 10. (a) EDS spectra of selected area on L samples surface; (b) EDS spectra of selected area on LI samples surface.

The EDS spectra of selected area on L and LI samples are shown in Fig.10. The carbon contents of selected regions were 8.51% on L surface and 22.75% on LI surface, respectively, indicating that a great deal of carbon gathered on nano-scale bulges. As shown in Fig. 10 (b), the nanoscale bulges of LI sample mainly contained carbon, oxygen, nickel and titanium with a relative concentration of 22.75%, 23.33%, 34.74%, and 19.18%, respectively. The atomic ratio of carbon to titanium was close to 1:1. Hence, it can be concluded that the main chemical composition of nanoscale bulges on LI sample after carbon ion implanting process was TiC, which had strong mechanical properties.

4.4 Analysis of abrasion stability

4.4.1 Evolution of surface morphology under abrasion treatment

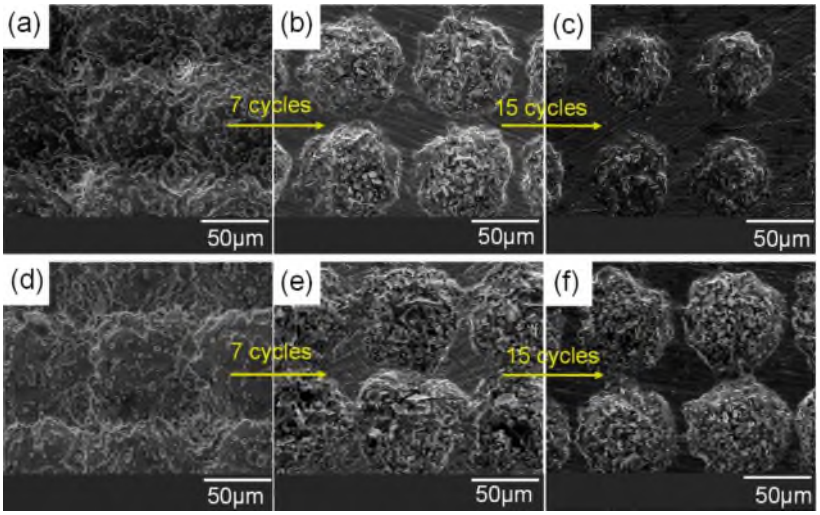

Figure 11. Surface morphology on L sample under (a) none abrasion cycle, (b) 7 times abrasion cycles and (c) 15 times abrasion cycles; Surface morphology on LI sample under (d) 0 time abrasion cycle, (e) 7 times abrasion cycles and (f) 15 times abrasion cycles

Fig. 11 showed the evolutions of surface morphology of L and LI samples under different abrasion cycles. It can be seen that rosette protrusions and spindrift shape ridges on both of L and LI samples' surfaces had been destroyed, and the surface morphology became flatter with the increase of abrasion. Meanwhile, the grooves became narrower and shallower. Compared with L samples, surface morphology of LI sample showed a tiny degeneration, presenting better mechanical abrasion resistance. This was because that titanium carbide formed on the surface of titanium alloy surface after carbon ion implantation, which obviously enhanced surface mechanical strength.

4.4.2 Evolution of surface chemical composition under abrasion treatment.

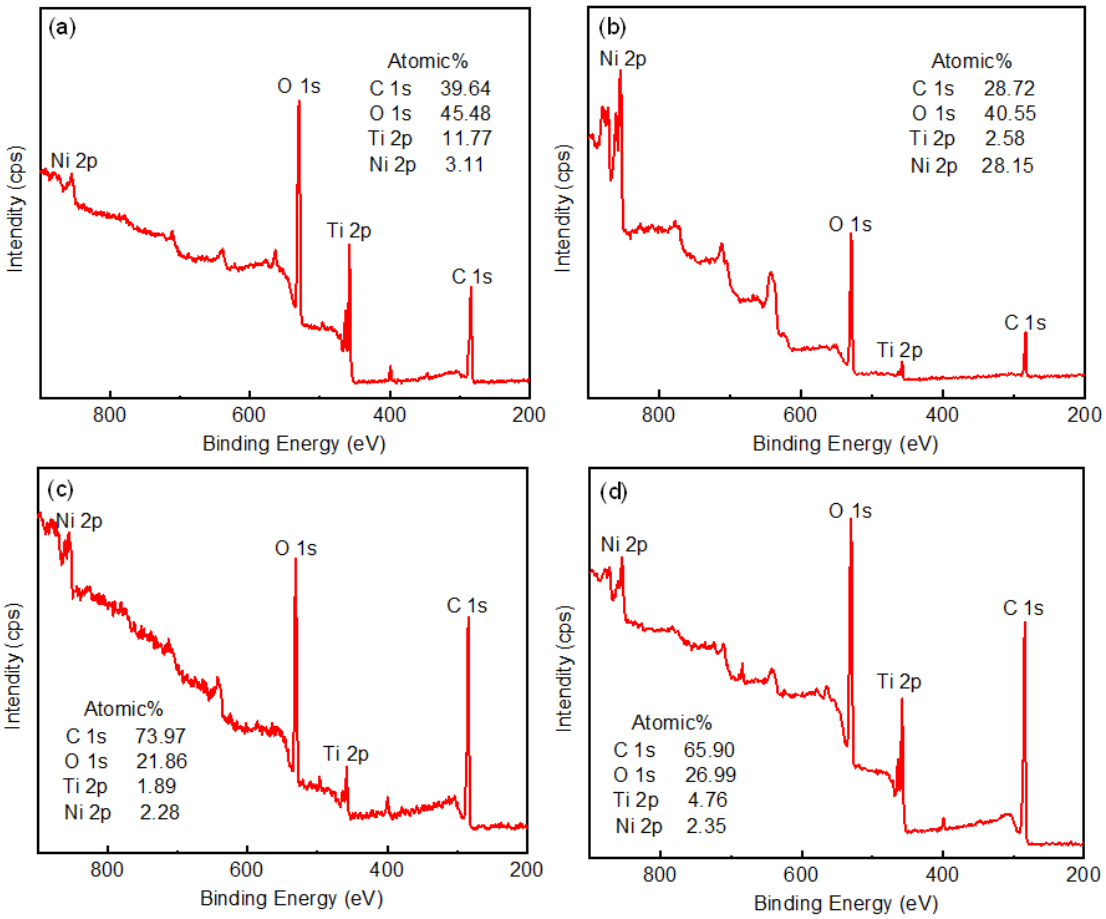

Figure 12. XPS spectra of L sample under (a) 7 times abrasion cycles and (b) 15 times abrasion cycles; XPS spectra of LI sample under (c) 7 times abrasion cycles and (d) 15 times abrasion cycles.

To explore the change of chemical composition with the increase of abrasion cycles, the corresponding chemical compositions of L and LI samples under 7 and 15 abrasion cycles were added in Fig. 12. Fig. 12 (a) and (b) demonstrated that the carbon content of L samples witnessed the continuous reducing: one was the decline from 59.21% to 39.64% after seven times abrasion and another decrease was from 39.64% to 28.72% after fifteen times abrasion. However, in terms of LI samples, the carbon decreased to 73.97% and 65.90% after seven and fifteen abrasion cycles, respectively. Compared with L samples, the downtrend on LI samples was relatively feebler, remaining higher content of carbon. Due to the reinforce effect of titanium carbide, fewer of the micro-nano particles that absorbed nonpolar groups of C-C(H) were removed off the surface, resulting in the higher content of carbonel ement.

4.4.2 Effect of abrasion treatment on surface wettability

The evolutions of WCAs on L and LI samples with different abrasion cycles were shown in Fig. 13 and the surface wettability was immediately measured after the cooling process in vacuum environment. According to the data curve, the WCAs of these two kinds of samples witnessed the continuous decline with the increase of abrasion number and the descent rate of WCAs on all samples gradually became slow because the surface morphology turned into flatter with the increment of friction cycles. As shown in Fig. 13, during the whole abrasion text, WCAs of the L samples declined from 147.5±2.1 ° to 105.3±1.7 °, however, the LI samples presented a tiny decrease from 155.5±2.0 ° to 129.7±2.3 °. These phenomena demonstrated that LI sample possessed superior wetting stability than L sample. Due to the strengthening effect of titanium carbide, fewer of the micro-nano particles and the absorbed nonpolar groups of C-C(H) were removed off the surface, resulting in the higher of surface non-polarity. As a result, the surface wettability on LI samples presented the tiny decline of WCAs. Therefore, carbon ion implantation distinctly improved the abrasion stability by improving mechanical intensity of micro-nano structures and reducing the cutting off of absorbed nonpolar carbonaceous matter.

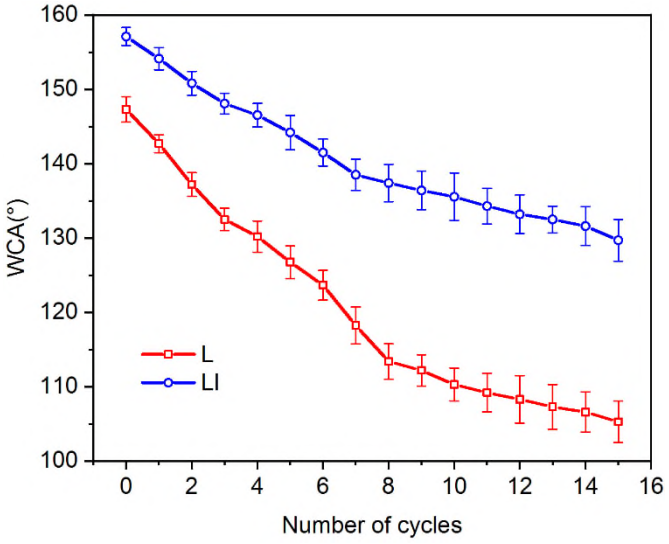

Figure 13. The revolution of WCAs on L and LI samples surface with different abrasion cycles.

4.5 Analysis of thermal stability

4.5.1 Evolution of surface morphology with different temperature

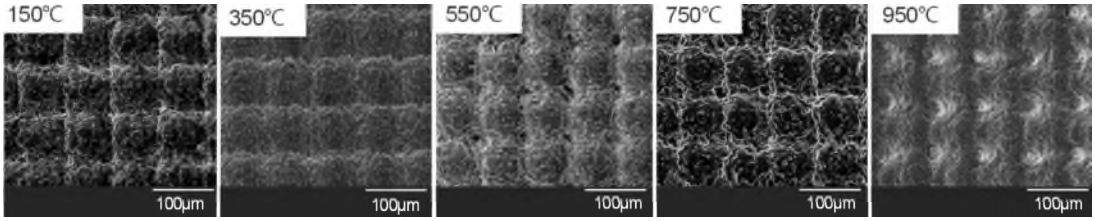

Figure 14. Evolution of surface morphology on L and LI surfaces with different temperatures.

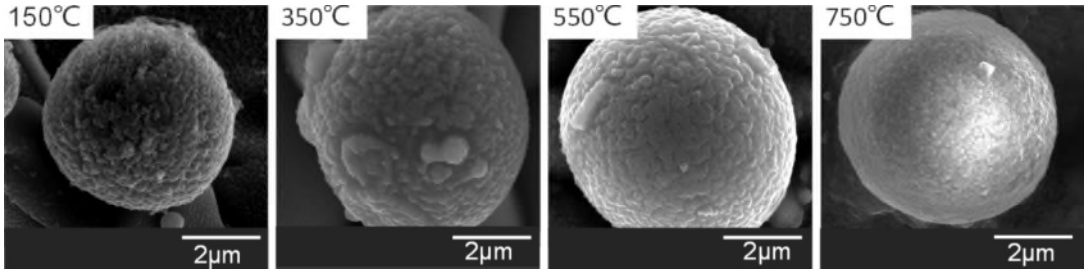

Figure 15. Revolution of nanoscale bulges on LI surface with different temperatures.

None significant differences were observed in micro-scale morphology among L and LI samples when heated at a certain temperature. Hence, Fig. 14 only presented one group images to show the evolution of surface morphology with different heating temperature. According to Fig. 14, surface morphology remained unchanged until 550 ℃. However, a flatter tendency appeared between 750 ℃ and 950 ℃ and the complex microstructure including grooves and droplet shape micro/nano-particles disappeared gradually. When the temperature came to 950 ℃, the microstructure was replaced by stratified structure absolutely. Fig. 15 showed the evolution of nanoscale bulges on LI sample at the corresponding temperature and the nanoscale bulges also witnessed a disappear process with the heating temperature going up. When the temperature came to 950 ℃, the nano-particles disappeared completely.

4.5.2 Effect of thermal treatment on surface wettability

In this section, to investigate the thermal stability of the investigated samples, the revolution of WCAs was evaluated in Fig. 16 and the surface wettability was immediately measured in vacuum environment after the cleaning and drying processes. It is obvious that all kinds of samples witnessed stabilization, dropping and increasing trend with the temperature going up from 50 ℃ to 950 ℃. As shown in Fig. 16 (a), the WCAs of L samples waved around 147° with the negligible tiny variation under 250 ℃, then it dropped to 23.2° sharply and lost hydrophobic performance at 300 ℃. With the

temperature going up, WCAs increased but still showed hydrophilicity. Fig. 16 (b) illustrated the LI surface kept super-hydrophobicity until 350 ℃ and then turned into hydrophobicity with the WCAs larger than 130 ° between 400 ℃ and 450 ℃. When the temperature exceeded 500 ℃, the surface presented hydrophilicity because the WCAs was no more than 90° and the WSA kept 180° in the meantime.

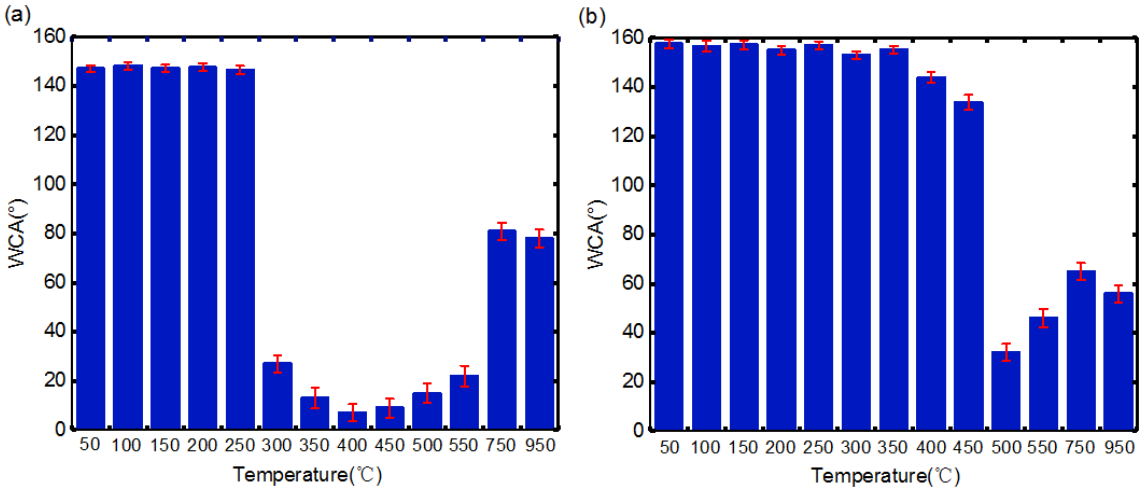

Figure 16. The revolution of WCAs on (a) L surfaces, (b) LI surfaces with different temperature.

According to Fig. 16 (a) the turning point temperature of L samples was at 300 ℃, below which the surface morphology had not started turning flatter. Therefore, it can be inferred that the change of wettability below 300℃ owed to the change of surface chemistry. To revealed the turning mechanism, the chemical composition before and after heating treatment under 300 ℃ was analyzed in Fig. 5 (b), Fig. 6 (b), Fig. 17 (a) and Fig. 17 (b), respectively. As far as L samples, the carbon content decreased to 18.16 ％. Besides, the concentration of polar functional group C-C(H) witnessed a sharp decrease from 72.02 ％ to 54.79 ％ after heat treatment, indicating that absorbed organic compounds were partly removed under 300 ℃. As a result, the surface un-polarity decreased with the growth of surface energy and therefore transformed from hydrophobicity to hydrophilicity.

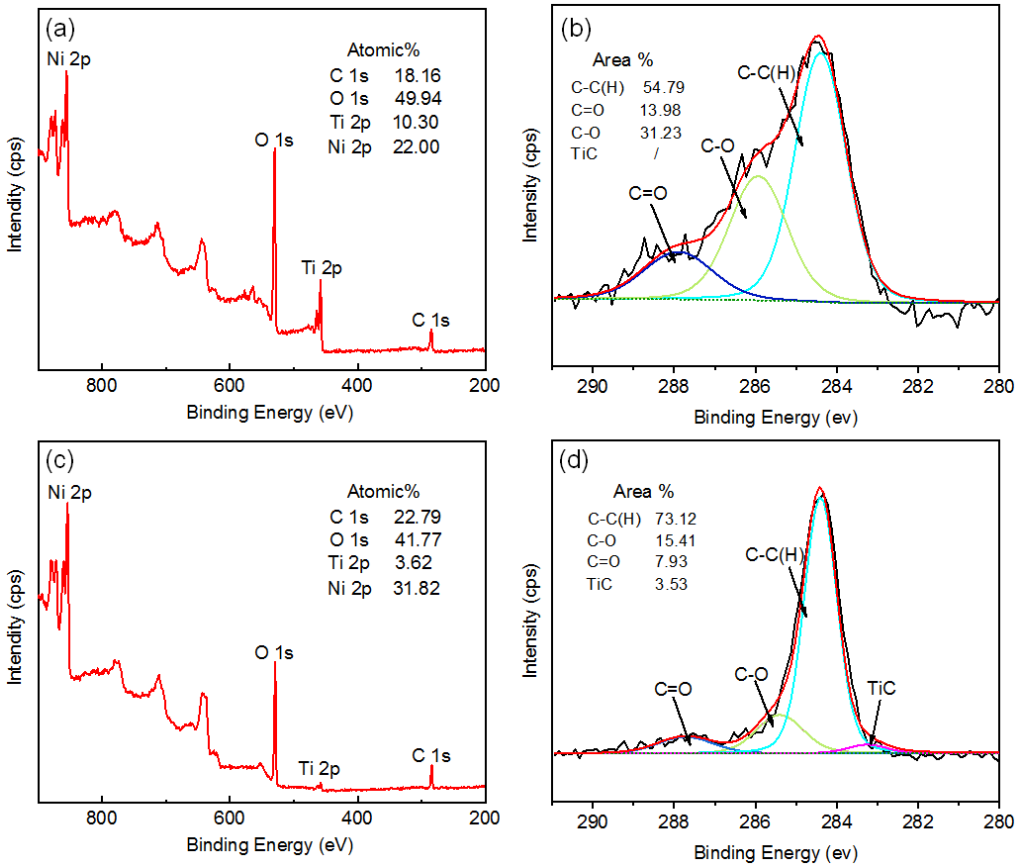

Figure 17. XPS spectra on heated L samples (a) and LI samples (c); the high-resolution of C 1s spectra on heated L samples (b) and LI samples (d) under 300℃.

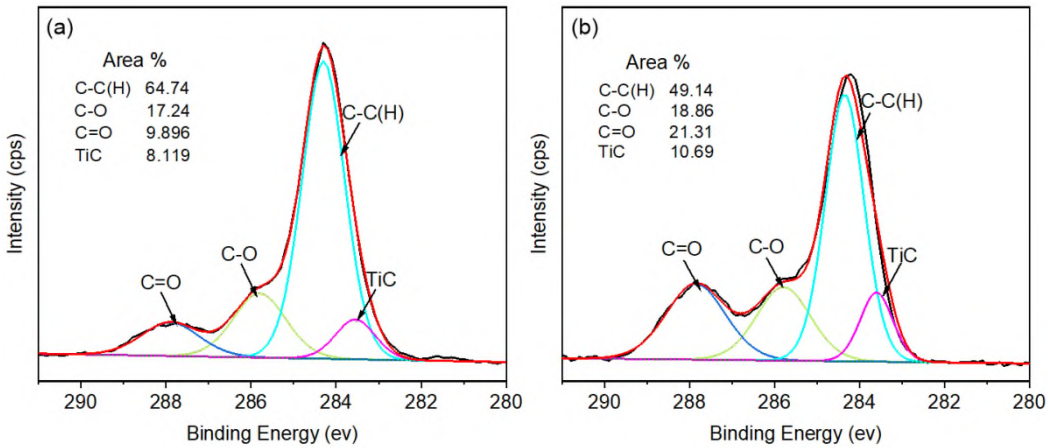

Figure 18. The high-resolution of C 1s spectra on heated LI samples under (a) 400℃ and (b) 500 ℃.

Praiseworthily, the carbon ion implanted surfaces (LI sample) kept super-hydrophobicity until 350℃ in Fig. 16 (b). Both XPS spectra and the high-resolution of C 1s spectra in Fig. 17 (c) and (d) revealed that the C-C(H) still remained the main concentration due to the tiny decrease from 85.76 % (as shown in Fig. 6 (d)) to 73.12 %, indicating enough absorbed organic compounds on the heated surface ensuring the low surface energy. Besides, the nano-scale bulges on micro-scale particle surface at the high temperature of 350 ℃ still strengthened the surface hydrophobic property. When the temperature came to 400 ℃, surface wettability turned form super-hydrophobicity to hydrophobicity. The high-resolution of C 1s spectra in Fig. 18 (a) demonstrated that the concentration of nonpolar functional group C-C(H) decreased to 64.74 %, which indicated the removing of the absorbed carbonaceous matter during the fading process of nanoscale bulges with the temperature going up. As a result, the surface polarity and energy increased. However, the non-polarity still occupied the dominance of surface, leading to formation of hydrophobic property under 400 ℃. On the contrary, it is regarded as that the fewer concentration of C-C(H) in Fig. 18 (b) was induced by the majority of C-C(H) abscission off the surface when the temperature came to 500 ℃, which resulted in the formation of polarity on surface. Hence, the surface wettability turned to hydrophilicity. When the temperature rose above 550 ℃, the nano-scale bulges obviously waned and the absorbed organic compounds were severely removed. Hence, the LI sample did not present super-hydrophobicity anymore. Above all, the thermal stability distinctly improved after carbon ion implantation.

5. Conclusions

In this work, the green and healthy super-hydrophobic surfaces have been fabricated on NiTi alloy surface by hybrid of nanosecond laser ablation and carbon ion implantation process. Compared with laser processing only, this fabricating method can effectively enhance hydrophobicity and shorten the transition time. As far as LI samples, the transformation from hydrophilicity to super-hydrophobicity only spent 16 hours, meanwhile, WCAs came to 156.2 ± 2.3°. However, the L samples took 35 days and the WCAs reached to 147.3 ± 2.3°. Above-mentioned advantageous effects benefited from carbon ion implantation were revealed in this paper. The surface morphology demonstrated many nano-scale bulges ranged from 100nm to 300nmvegetated on micron particle surfaces (the lotus-leaf-like

hierarchical structures) after carbon ion implantation. According to tip discharge principle, a great deal of charges gathered on the top of nano-scale bulges, which obviously enhanced surface adsorptive property. As a result, the absorbing process of organic compounds enhanced in terms of quantity and efficiency. This hybrid method of nanosecond laser irradiation and carbon ion implantation is low-cost, offering a high-efficient way for quantity fabrication of lotus-like hierarchical surface. In addition, the elaborate experiments were carried out to explore abrasion stability and thermal stabilities of investigated samples, and the mechanism was also discussed to make a better understanding between modified hydrophobic surface and stability, which will raise the promising prospects of nitinol for application.

Acknowledgements

This work received funding support from National Key R&D Program of China [Nos. 2017YFB1104700] and the National Natural Science Foundations of China (Nos. 51675371, 51675376 and 51675367).

References

[1] H.K. Raut, A.S. Ranganath, A. Baji, K.L. Wood, Bio-inspired hierarchical topography for texture driven fog harvesting, Applied Surface Science. 465 (2019), 362-368.

[2] H. Li, S. Yu, A robust super-hydrophobic surface and origins of its self-cleaning properties, Applied Surface Science. 420 (2017), 336-345.

[3] C.J. Yang, X.B. Jing, F.J. Wang, K.F. Ehmann, Y.L. Tian, Z.H. Pu, Fabrication of controllable wettability of crystalline silicon surfaces by laser surface texturing and silanization, Applied Surface Science. 497 (2019), 143805.

[4] Z. Yang, X.P. Liu, Y.L. Tian, Hybrid Laser Ablation and Chemical Modification for Fast Fabrication of Bio-inspired Super-hydrophobic Surface with Excellent Self-cleaning, Stability and Corrosion Resistance, Journal of Bionic Engineering. 16 (2019), 16-26.

[5] Z. Yang, Y.L. Tian, C.J. Yang, Modification of wetting property of Inconel 718 surface by nanosecond laser texturing, Applied Surface Science. 414 (2017), 313-324.

[6] Z. Yang, X.P. Liu, Y.L. Tian, A Contrastive Investigation on Anticorrosive Performance of Laser-induced Super-hydrophobic and Oil-infused Slippery Coatings, Progress in Organic Coatings, 138 (2020), 105313.

[7] Y. Liu, S.Y. Li, J.J. Zhang, J.A. Liu, Z.W. Han, L.Q. Ren, Corrosion inhibition of biomimetic superhydrophobic electrodeposition coatings on copper substrate, Corrosion Science. 94 (2015), 190-196.

[8] Z. Yang, X.P. Liu, Y.L. Tian, Fabrication of Super-hydrophobic Nickel Film on Copper Substrate with Improved Corrosion Inhibition by Electrodeposition Process, Colloids and Surfaces A. 560 (2019), 205-212.

[9] T.S. Tang, Q. Liu, J.Y. Liu, W.L. Yang, R.R. Chen, X.Y. Jing, T. Kazunobu, J. Wang, Fabrication of super slippery sheet-layered and porous anodic aluminium oxide surfaces and its anticorrosion property, Applied Surface Science. 355 (2015), 495-501.

[10] C.H. Kung, B. Zahiri, P.K. Sow, W. Mérida, On-demand oil-water separation via low-voltage wettability switching of core-shell structures on copper substrates, Applied Surface Science. 444 (2018), 15-27.

[11] F.J. Peaudecerf, J.R. Landel, R.E. Goldstein, P. Luzzatto-Fegiz, Traces of surfactants can severely limit the drag reduction of superhydrophobic surfaces, Proceedings of the National Academy of Sciences of the United States of America. 114 (2017), 7254-7259.

[12] X.F. Liao, H.Q. Li, L. Zhang, X.J. Su, X.J. Lai, X.R. Zeng, Superhydrophobic mGO/PDMS hybrid coating on polyester fabric for oil/water separation, Progress in Organic Coatings. 115 (2018), 172-180.

[13] B.X. Zheng, W.J. Wang, G.D. Jiang, X.S. Mei, Fabrication of Broadband Antireflective Black Metal Surfaces with Ultra-light-trapping Structures by Picosecond Laser Texturing and Chemical Fluorination, Applied Physics. B: Laser and Optics. 122, (2016), 1-15.

[14] B. Liu, W.J. Wang, G.D. Jiang, X.S. Mei, Study on hierarchical structured PDMS for surface super-hydrophobicity using imprinting with ultrafast laser structured models, Applied Surface Science. 354 (2016), 528-538.

[15] J.L. Yong, F. Chen, Q. Yang, J. Huo, X. Hou, Superoleophobic surfaces, Chemical Society Reviews. 46 (14) (2017), 4168-4217.

[16] C.J. Yang, Y.C. Zhao, Y.L. Tian, F.J. Wang, X.P. Liu, X.B. Jing, Fabrication and Stability Investigation of Bio-Inspired Superhydrophobic Surface on Nitinol Alloy, Colloids and Surfaces A. 567 (2019), 16-26.

[17] Y. Wan, L. Xu, Z. Liu, H. Yu, Fabrication of a super-amphiphobic aluminium alloy surface via wire electrical discharge machining and chemical etching technology, Micro and Nano Letters, 12 (2017), 175-178.

[18] X. Li, X. Yu, C. Cheng, L. Deng, M. Wang, X. Wang, Electrospun superhydrophobic organic/inorganic composite nanofibrous membranes for membrane distillation, ACS Applied Materials & Interfaces. 7 (2015), 21919-21930.

[19] N. Lv, X. Wang, S. Peng, H. Zhang, L. Luo, Study of the kinetics and equilibrium of the adsorption of oils onto hydrophobic jute fiber modified via the sol-gel method, International Journal of Environmental Research & Public Health. 15 (2018), 969.

[20] S. Bauer, J. Park, K.V.D. Mark, P. Schmuki, Improved attachment of mesenchymal stem cells on super-hydrophobic TiO2 nanotubes, Acta Biomaterialia. 4 (2008), 1576-1582.

[21] C.K. Söz, E. Yilgör, I. Yilgör, Influence of the average surface roughness on the formation of superhydrophobic polymer surfaces through spin-coating with hydrophobic fumed silica, Polymer. 62 (2015), 118-128.

[22] Z. Yang, Y.L. Tian, Y.C. Zhao, C.J. Yang, Study on the Fabrication of Super-Hydrophobic Surface on Inconel Alloy via Nanosecond Laser Ablation, Materials. 12 (2019).

[23] A.F. Pan, W.J. Wang, X.S. Mei, K.D. Wang, X.B. Wang, Rutile TiO 2 Flocculent Ripples with High Antireflectivity and Superhydrophobicity on the Surface of Titanium under 10 ns Laser Irradiation without Focusing, Langmuir. 33 (2017), 9530-9538.

[24] J. Li, W.J. Wang, X.S. Mei, A.F. Pan, X.F. Sun, B. Liu, J.L. Cui, Artificial Compound Eyes Prepared by a Combination of Air-Assisted Deformation, Modified Laser Swelling, and Controlled Crystal Growth, ACS NANO. 13 (2019), 114-124.

[25] C.J. Yang, M. Wang, Z. Yang, D.W. Zhang, Y.L. Tian, X.B. Jing, X.P. Liu, The investigation of effects of acid, alkali and salt solution on fluorinated super-hydrophobic surface, Langmuir, 35 (2019), 17027-17036.

[26] C.W. Chan, S. Lee, G. Smith, G. Sarri, C. H. Ng, A. Sharba, H.C. Man, Enhancement of wear and corrosion resistance of beta titanium alloy by laser gas alloying with nitrogen, Applied Surface Science. 367 (2016), 80-90.

[27] H.J. Rack, J.I. Qazi, Titanium alloys for biomedical applications, Advances in Metallic Biomaterials. (2015), 179-213.

[28] A. Raffaella, T. Francesco, R.V.V. Petrescu, F.I.T. Petrescu, A. Mateus, Y. Guan, C.A. Antonio, Biomechanically inspired shape memory effect machines driven by muscle like acting niti alloys. American Journal of Applied Sciences, 13 (2016), 1264-1271.

[29] Y. Wang, H. Yu, C. Chen, Z. Zhao, Review of the biocompatibility of micro-arc oxidation coated titanium alloys, Materials & Design. 85 (2015), 640-652.

[30] Y.L. Tian, Y.C. Zhao, C.J. Yang, F.J. Wang, X.P. Liu, X.B. Jing, Fabrication of bio-inspired nitinol alloy surface with tunable anisotropic wetting and high adhesive ability, Journal of Colloid and Interface Science. 527 (2018), 328-338.

[31] C.R. Knick, D. Sharar, A. Wilson, G. Smith, C.J. Morris, High frequency, low power, electrically actuated shape memory alloy (SMA) MEMS bimorph thermal actuators, Journal of Micromechanics and Microengineering. 29 (2019), 075005.

[32] S.K. Satpute, N.S. Mone, P. Das, I.M. Banat, A.G. Banpurkar, Inhibition of pathogenic bacterial biofilms on PDMs based implants by L. acidophilus derived biosurfactant, BMC Microbiology. 19 (39) (2019).

[33] E. Fadeeva, V.K. Truong, M. Stiesch, B.N. Chichkov, R.J. Crawford, J. Wang, E.P. Ivanova, Bacterial retention on superhydrophobic titanium surfaces fabricated by femtosecond laser ablation, Langmuir. 27 (6) (2011), 3012-3019.

[34] H. Gu, S.W. Lee, S.L. Buffington, J.H. Henderson, D. Ren, On demand removal of bacterial biofilms via shape memory activation, ACS Applied Materials & Interfaces. 8 (2016), 21140-21144.

[35] W.J. Wang, J. Li, R.H. Li, B.Q. Li, X.S. Mei, X.F. Sun, Fabrication of Hierarchical Micro/Nano Compound Eyes, Applied Material and Interface. 11 (2019), 34507-34516.

[36] E. Fadeeva, V.K. Truong, M. Stiesch, B.N. Chichkov, R.J. Crawford, J. Wang, E. Ivanova, Bacterial retention on superhydrophobic titanium surfaces fabricated by femtosecond laser ablation, Langmuir. 27 (2011), 3012-3019.

[37] M.A. Hasan, S. Rashmi, A.C.M. Esther, P.Y. Bhavanisankar, B.N. Sherikar, N. Sridhara, D. Arjun, Evaluations of silica aerogel-based flexible blanket as passive thermal control element for spacecraft applications, Journal of Materials Engineering and Performance. 27 (2018), 1265-1273.

[38] J.B. Boreyko, Y. Zhao, C.H. Chen, Planar Jumping-Drop Thermal Diodes, Applied Physics Letters. 99 (2011), 234105.

[39] G.R. Yenni, A. Ambirajan, C. Balaji, S.P. Venkateshan, Emissivity estimation of spacecraft thermal control surfaces at cryogenic temperatures - a novel experimental approach, Heat and Mass Transfer. 55 (2019), 1465-1476.

[40] J.A. Supowit, C.H. Baker, B. Zhao, J. McHale, R. Miller, Thermal cycle testing of titanium superhydrophobic surfaces for a spacecraft jumping roplet thermal diode, 2018 Jt. Thermophys. Heat Transf. Conf. American Institute of Aeronautics and Astronautics, Reston, Virginia.

[41] H.Y. Shen, J.Z. Cao, J. Jiang, J.Q. Xu, Antiweathering properties of a thermally treated wood surface by two-step treatment with titanium dioxide nanoparticle growth and polydimethylsiloxane coating, Progress in Organic Coatings. 125 (2018), 1-7

[42] S. Tuerk, A. Jupe, R. Viga, H. Vogt, Analysis and simulation of super-hydrophobic layers for microfluidic applications, Konferenz: Mikro-Nano-Integration - 7. GMM-Workshop. 22.10.2018 - 23.10.2018 in Dortmund, Deutschland Micro-Nano-Integration. 92 (2018), 33-37.

[43] L. Zhang, L. Zhang, Y. Yang, W. Zhang, H. Lv, F. Yang, C. Lin, P. Tang, Inhibitory effect of super-hydrophobicity on silver release and antibacterial properties of super-hydrophobic Ag/TiO2 nanotubes, Journal of Biomedical Materials Research Part B Applied Biomaterials. 104 (2016), 1004-1012.

[44] C. Xia, S. Qian, D. Wang, X.Y. Liu, Properties of Carbon Ion Implanted Biomedical Titanium, Ion implantation. 53 (2017), 1393-1401.

[45] K. Yin, H. Du, Z. Luo, X. Dong, J.A. Duan, Multifunctional micro/nano-patterned PTFE nearsuperamphiphobic surfaces achieved by a femtosecond laser, Surface & Coatings Technology. 345 (2018), 53-60.

[46] R.N. Wenzel, Resistance of solid surfaces to wetting by water, Journal of Industrial and Engineering Chemistry. 28 (1936) 988–994.

[47] B. Bhushan, Y.C. Jung, Wetting, Adhesion and friction of superhydrophobic and hydrophilic leaves and fabricated micro/nanopatterned surfaces, Journal of Physics: Condensed Matter. 20 (2008), 225010.

[48] Z. Yang, Y. L. Tian, X. P. Liu, Insights into the wettability transition of nanosecond laser ablated surface under ambient air exposure, Journal of Colloid and Interface Science. 533 (2019) 268-277.

[49] K.C. Hass, W.F. Schneider, A. Curioni, W. Andreoni, The chemistry of water on alumina surfaces: reaction dynamics from first principles, Science 282 (1998) 265–268.

[50] D. Argyris, P.D. Ashby, A. Striolo, Structure and orientation of interfacial water determine atomic force microscopy results: insights from molecular dynamics simulations, ACS Nano 5 (2011) 2215–2223.

[51] M.R. Gorji, S. Sanjabi, Surface free energy of TiC layers deposited by electrophoretic deposition (EPD), American Institute of Physics Conference Series. (2018).

[52] D. Saha, H.A. Greppe, 5 – Adsorption properties of activated carbon fibers, Activated Carbon Fiber and Textiles. (2017), 143-165.

[53] R.S. Summers, P.V. Roberts, Activated carbon adsorption of humic substances: II. Size exclusion and electrostatic interactions, Journal of Colloid and Interface Science. 122 (1988), 382-397.

[54] F.J.G. Heyes, H.P. Hodson, G.M. Dailey, The Effect of Blade Tip Geometry on the Tip Leakage Flow in Axial Turbine Cascades, Journal of Turbomachinery-Transactions of the Asme. 114 (1991), 643-651.